

AGN populations in the local universe: their alignment with the main-sequence, characteristics of their stellar populations, accretion efficiency, and the impact of AGN feedback

G. Mountrichas¹, A. Ruiz², I. Georgantopoulos², E. Pouliaxis², A. Akylas² and E. Drigga²

¹ Instituto de Fisica de Cantabria (CSIC-Universidad de Cantabria), Avenida de los Castros, 39005 Santander, Spain e-mail: gmountrichas@gmail.com

² National Observatory of Athens, Institute for Astronomy, Astrophysics, Space Applications and Remote Sensing, Ioannou Metaxa and Vasileos Pavlou GR-15236, Athens, Greece

May 21, 2024

ABSTRACT

In this study, we utilize a sample of 338 galaxies within the redshift range of $0.02 < z < 0.1$, drawn from the Sloan Digital Sky Survey (SDSS), for which there are available classifications, based on their emission line ratios. We, further, identify and select Compton-thick (CT) AGN through the use of X-ray and infrared luminosities at $12 \mu\text{m}$. We construct the spectral energy distributions (SEDs) for all sources and fit them using the CIGALE code to derive properties related to both the AGN and host galaxies. Employing stringent criteria to ensure the reliability of SED measurements, our final sample comprises 14 CT AGN, 118 Seyfert 2 (Sy2), 82 composite, and 124 LINER galaxies. Our analysis reveals that, irrespective of their classification, the majority of the sources lie below the star-forming main-sequence (MS). Additionally, a lower level of AGN activity is associated with a closer positioning to the MS. Utilizing the D_n4000 spectral index as a proxy for the age of stellar populations, we observe that LINERs exhibit the oldest stellar populations compared to other AGN classes. Conversely, CT sources are situated in galaxies with the youngest stellar populations. Furthermore, LINER and composite galaxies tend to show the lowest accretion efficiency, while CT AGN, on average, display the most efficient accretion among the four AGN populations. Our findings are consistent with a scenario in which the different AGN populations might not originate from the same AGN activity burst. Early triggers in gas rich environments can create high accretion rate SMBHs leading to a progression from CT to Sy2, while later triggers in gas poor stages result in low accretion rate SMBHs like those found in LINERs.

1. Introduction

In the realm of active galactic nuclei (AGN), the local Universe presents a diverse population of galaxies hosting different AGN classes, each characterized by distinct observational features. Among these classes, there are LINERs (Low-Ionization Nuclear Emission-line Regions), Seyferts, and composite galaxies that consist of both AGN and star-forming systems, each offering valuable insights into the intricate interplay between supermassive black holes (SMBHs) and their host galaxies. Understanding the properties and behaviours of these AGN classes is crucial for unraveling the mechanisms that drive their activity and influence the evolution of their host systems.

Investigating the star formation rate (SFR) and stellar mass, M_* of galaxies hosting AGN provides a crucial contextual framework for comprehending their evolutionary trajectories (e.g., Rosario et al. 2012; Santini et al. 2012; Rosario et al. 2013; Mullaney et al. 2015; Masoura et al. 2018; Bernhard et al. 2019; Mountrichas et al. 2021a,b; Koutoulidis et al. 2022; Pouliaxis et al. 2022; Mountrichas et al. 2023; Mountrichas & Buat 2023; Mountrichas et al. 2024a). These parameters offer essential clues about the ongoing astrophysical processes within these galaxies, shedding light on the co-evolution of AGN and their host galaxies. LINER, Seyferts and composite galaxies, serve as unique laboratories to explore the inter-dependencies between AGN activity, star formation, and the overall stellar content of their host systems.

The study of stellar populations across the different AGN populations offers a glimpse into the historical star formation

activity within these systems (e.g., Kauffmann et al. 2003; Kauffmann et al. 2003; Kewley et al. 2006; Mountrichas et al. 2022b; Georgantopoulos et al. 2023). Utilizing parameters like the D_n4000 spectral index, which serves as a proxy for the age of stellar populations, enables researchers to unravel the past evolutionary paths of these galaxies.

The Eddington ratio, denoted as n_{Edd} , emerges as a pivotal parameter in quantifying the accretion efficiency of AGN. Defined as the ratio of the bolometric luminosity to the Eddington luminosity (i.e., the maximum luminosity an AGN can emit; $L_{Edd} = 1.26 \times 10^{38} M_{BH}/M_{\odot} \text{ erg s}^{-1}$, where M_{BH} is the mass of the SMBH), n_{Edd} provides insights into the balance between radiation pressure and gravitational forces around the SMBH. Examining the n_{Edd} values for different AGN populations allows for a comparative analysis of the evidence indicates that the different types of AGN we've examined may result from distinct phases of AGN activity. For example, if a supermassive black hole (SMBH) becomes active early in a galaxy's evolution, when there's plenty of gas, it might exhibit a high accretion rate, appearing as a Seyfert 2 (Sy2) and potentially transitioning from Compton-thick (CT) to Sy2. On the other hand, if the AGN activity begins later in the galaxy's timeline when gas is less abundant, the SMBH would likely have a lower accretion rate, leading to a Low-Ionization Nuclear Emission-line Region (LINER).eir accretion processes, offering a deeper understanding of the diverse ways in which AGN interact with their environments (e.g., Kewley et al. 2006; Georgantopoulos et al. 2023; Mountrichas & Georgantopoulos 2024; Mountrichas et al. 2024b).

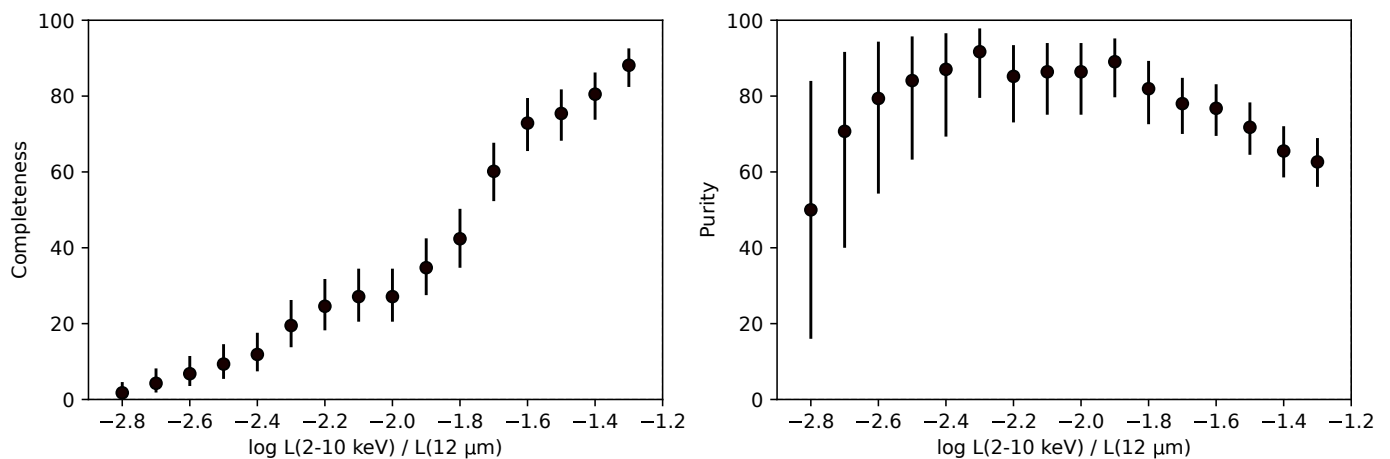


Fig. 1: Completeness (left) and purity (right) for CT AGN in the BASS sample depending on different selection criteria based on X-ray-to-MIR-luminosity ratio.

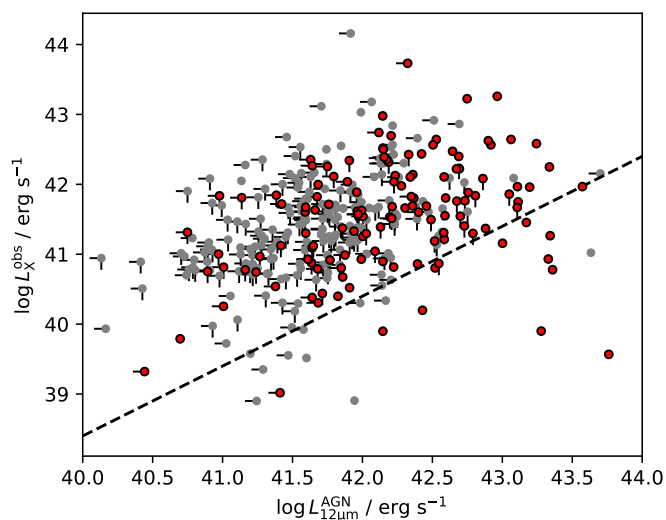


Fig. 2: AGN luminosity at $12\ \mu\text{m}$, as estimated by CIGALE, versus observed X-ray luminosity in the 2-10 keV band for our sample of local SDSS AGN. Grey circles correspond to LINER/Composite objects, red circles are Seyfert 2 galaxies. Symbols marked with a horizontal and/or vertical bar show upper-limits in the $12\ \mu\text{m}$ and/or X-ray luminosity, respectively. The black, dashed line shows $\log(L_X^{\text{obs}}/L_{12\ \mu\text{m}}^{\text{AGN}}) = -1.6$.

Previous studies have found that LINER galaxies tend to have higher M_* , redder optical colors and higher black hole masses compared to Seyferts (e.g. [Smolčić 2009](#)). LINERs also are more dusty and more concentrated than Seyferts, although, these differences could be, mainly, due to the different n_{Edd} of the AGN populations, with LINERs to be dominant at low n_{Edd} and Seyferts dominant at high n_{Edd} (e.g., [Kewley et al. 2006](#)). Seyferts also appear to reside in dark matter holes with lower mass compared to LINERs ([Constantin & Vogeley 2006](#)). For an in-depth overview of the various AGN populations, refer to [Heckman & Best \(2014\)](#).

In this work, we use galaxies from the Sloan Digital Sky Survey (SDSS; [Almeida et al. 2023](#)) for which there are available classifications, based on their emission lines. Specifically, sources are categorized into Seyfert 2 (Sy2), composite and

LINER galaxies. Furthermore, we identify and select Compton-thick (CT) AGN using their X-ray and infrared luminosities at $12\ \mu\text{m}$. The data and the CT selection criteria are described in Sect. 2. In Sect. 3, we describe the process we follow to fit the spectral energy distributions (SEDs) of all the sources, using the CIGALE code, as well as the strict selection criteria we apply to select galaxies with robust SED fitting measurements. We perform a comprehensive investigation into SFR, M_* , accretion efficiency and stellar populations to decipher the intricate connections between AGN activity and the broader processes governing galaxy evolution in the local universe. The results appear in Sect. 4. In Sect. 5, we discuss our main findings and compare them with prior studies. Finally, Sect. 6 presents a summary of our main findings.

2. Data

2.1. Sample selection

Our goal is to select a sample of low redshift, obscured AGN observed in X-rays while minimizing the contamination of star-forming galaxies. To this end we follow the criteria presented in [Zhang \(2023\)](#) for selecting type 2 AGN in the SDSS: we selected all objects in the SDSS-DR18 ([Almeida et al. 2023](#)) spectroscopic database (specObj table) that according to the SDSS pipeline have been classified as galaxies and with subclass AGN. We restrict our sample to galaxies with redshift below 0.1. In order to exclude local galaxies with a large extension where the SDSS photometry is highly unreliable, we imposed an additional redshift cut of $z > 0.02$ (with this limit the spectrograph fiber covers $\gtrsim 1$ kpc of the nuclear region). We also selected only objects with good quality spectrum, i.e. with a median signal-to-noise ratio larger than 10 and no warnings in the estimated redshift. Finally, we kept only objects with a primary entry in the photometric database of SDSS and included in the Portsmouth catalogue of stellar kinematics and emission-line flux measurements ([Thomas et al. 2013](#)). This catalogue models the SDSS spectrum to derive the emission line properties and gives a reliable spectral classification (Seyfert, LINER, Composite, etc) based on BPT diagrams for each galaxy.

The final query that reflects this selection is:

```
SELECT * FROM specObj AS sp
JOIN PhotoObj AS ph
```

Table 1: Models and the values for their free parameters used by X-CIGALE for the SED fitting of our galaxy sample.

Parameter	Model/values
Star formation history: delayed model with recent, constant burst/quench	
Age of the main population	5000, 7000, 9000, 10000, 11000, 12000 Myr
e-folding time	1000, 3000, 5000, 7000, 9000, 10000, 11000, 12000 Myr
Age of the burst/quench	50, 100 Myr
Ratio of the SFR after/before the burst/quench episode	0.01, 0.2, 0.8, 0.9, 1.0, 1.005, 1.015, 1.05, 1.10, 1.15, 1.20
Simple Stellar population: Bruzual & Charlot (2003)	
Initial Mass Function	Salpeter
Metallicity	0.02 (Solar)
Galactic dust extinction	
Dust attenuation law	Charlot & Fall (2000)
Reddening A_V in the ISM	0.001, 0.1, 0.2, 0.3, 0.4, 0.5, 0.6, 0.8, 1.0, 1.5
Galactic dust emission: Dale et al. (2014)	
α slope in $dM_{dust} \propto U^{-\alpha} dU$	2.0
AGN module: SKIRTOR	
Torus optical depth at 9.7 microns $\tau_{9.7}$	3, 7, 11
Torus density radial parameter p ($\rho \propto r^{-p} e^{-q \cos(\theta) }$)	1.0
Torus density angular parameter q ($\rho \propto r^{-p} e^{-q \cos(\theta) }$)	1.0
Angle between the equatorial plan and edge of the torus	40°
Ratio of the maximum to minimum radii of the torus	20
Viewing angle	50°, 70°, 90°(type 2)
Accretion disk spectrum	Schartmann (2005)
AGN fraction	0.0, 0.01, 0.1, 0.2, 0.3, 0.4, 0.5, 0.6, 0.7, 0.8, 0.9
Extinction law of polar dust	SMC
$E(B - V)$ of polar dust	0.0, 0.2, 0.4
Temperature of polar dust (K)	100
Emissivity of polar dust	1.6

Notes. For the definitions of the various parameters, see Sect. 3.1.

```

ON sp.bestObjID=ph.objID
JOIN emissionLinesPort AS ln
ON sp.specObjID=ln.specObjID
WHERE
sp.class='galaxy' AND sp.subclass='AGN'
AND (sp.z BETWEEN 0.02 AND 0.1)
AND sp.zwarning=0 AND sp.snmedian>10

```

This query returns a total of 7382 sources in the SDSS-DR18 database. In order to select sources observed in X-rays, we query the position of each galaxy in the RapidXMM database (Ruiz et al. 2022). This system provides X-ray flux upper-limits for all positions in the sky that have been observed by XMM-Newton. As of May 2023¹, we found 479 objects, out of our initial 7382 galaxies, in fields observed by XMM-Newton. Out of these 479 sources, 210 have a counterpart within 5 arcsec in the 4XMM-DR13 catalogue (Webb et al. 2020). The 4XMM-DR13 catalogue was built using XMM-Newton observations released up to 2022 December 31st. Our sample contains sources in 22 observations that were not included in the 4XMM-DR13. For these cases we used the X-ray source catalogues generated by the XMM-Newton pipeline, available in the archive, finding six additional sources with X-ray counterparts. In total, about 45 per cent (216 sources out of 479 sources) of our final sample is detected in X-rays.

¹ XMM-Newton observations are ingested into the RapidXMM system when the data becomes public, so queries at a later date can give a larger number.

2.2. Photometry

In order to perform the SED analysis described in Sect. 3.1, we need to build SEDs with good photometric coverage. In the ultra-violet (UV), we search for counterparts in the Revised Catalog for the GALEX All-Sky Imaging Survey (GALEX-AIS, Bianchi et al. 2017). In the mid-infrared (MIR) regime, we used the AllWISE Catalog Cutri et al. (2013). For the near-infrared (NIR) photometry, we relied on three catalogues. Most of our sources have counterparts in the 2MASS Extended Source Catalog (2MASS-XSC, Skrutskie et al. 2006). When no counterpart was found in the 2MASS-XSC, we used the UKIDSS-DR11plus Large Area survey catalog (UKIDSS-LAS, Lawrence et al. 2007) if that sky region was covered by this survey, otherwise we search for a counterpart in the 2MASS Point Source Catalog (2MASS-PSC, Skrutskie et al. 2006).

Given the low redshift of our selected sample, most of our sources are extended sources, clearly resolved in the optical and NIR bands. For a correct estimation of the galaxy properties we need to select measurements of the magnitudes that recover the emission of the whole galaxy. We used Petrosian magnitudes for the five SDSS bands (u, g, r, i, z), as recommended for photometry of nearby galaxies. We used the 'best' FUV and NUV GALEX magnitudes as recommended in the AIS catalog documentation. For sources with 2MASS-XSC photometry we used the isophotal J, H and K magnitudes. In the case of UKIDSS-LAS, we used the Petrosian magnitudes for the J, H and K bands. In AllWISE, we used the elliptical aperture magnitudes for the four WISE bands (W1, W2, W3, W4) when available, otherwise we used the profile-fitting magnitudes. We visually inspected the images in the different bands and the constructed SEDs to check

Table 2: Number of sources included within each AGN population considered in our analysis

AGN population	number of sources
Sy2 (no CT)	118
Composite	82
LINERS	124
CT	14

that the different apertures used for measuring the magnitudes covered the same region of the galaxy.

3. Analysis

3.1. Galaxy properties

To compute the properties of AGN and their host galaxies (e.g., AGN bolometric luminosity, SFR, M_*), we employ SED fitting through the CIGALE algorithm (Boquien et al. 2019; Yang et al. 2020, 2022). We adhere to the same templates and parametric grid in the SED fitting process as utilized in prior works (e.g. Koutoulidis et al. 2022; Mountrichas et al. 2022c). In summary, the galaxy component is modeled using a delayed Star-Formation History (SFH) model with a functional form $SFR \propto t \times \exp(-t/\tau)$. A continuous star-formation period of 50 Myr is incorporated as a star-formation burst (Małek et al. 2018; Buat et al. 2019). Stellar emission is modeled using the single stellar population templates of Bruzual & Charlot (2003), attenuated in accordance with the Charlot & Fall (2000) attenuation law. To model nebular emission, CIGALE adopts nebular templates based on Villa-Velez et al. (2021). The emission from dust heated by stars is modeled following Dale et al. (2014), excluding any AGN contribution. The AGN emission is included using the SKIRTOR models of Stalevski et al. (2012, 2016). The parameter space employed in the SED fitting process is presented in Table 1.

3.2. Reliability criteria

To ensure the reliability of our analysis, we implement selection criteria akin to those employed in prior studies (e.g., Mountrichas et al. 2022a,b; Buat et al. 2021; Pouliaxis et al. 2022; Mountrichas & Buat 2023). Specifically, in order to exclude sources with unreliable SED fitting measurements and host galaxy information, we set a reduced χ^2 threshold of $\chi_r^2 < 5$ (e.g., Masoura et al. 2018; Buat et al. 2021). This criterion led to the exclusion of six sources from our dataset. Additionally, we omit systems for which the CIGALE algorithm could not constrain the SFR and M_* . For this purpose, we leverage the two values provided by CIGALE for each estimated galaxy property. One value corresponds to the best model, while the other (bays) represents the likelihood-weighted mean value. A substantial disparity between these two calculations implies a complex likelihood distribution and significant uncertainties. Consequently, we only incorporate sources in our analysis that satisfy the conditions $\frac{1}{5} \leq \frac{SFR_{best}}{SFR_{bays}} \leq 5$ and $\frac{1}{5} \leq \frac{M_{*,best}}{M_{*,bays}} \leq 5$, where SFR_{best} and $M_{*,best}$ are the best-fit values of SFR and M_* , respectively and SFR_{bays} and $M_{*,bays}$ are the Bayesian values estimated by CIGALE.

There are 338 sources that meet the specified criteria. Among these sources we identify and select 14 CT AGN candidates (see next section). From the remaining 324 galaxies, 118 are classi-

fied as Sy2, 82 as composite and 124 as LINER galaxies, based on the Portsmouth catalogue (Thomas et al. 2013). These are the sources used in our analysis (Table 2).

3.3. Selection of Compton-Thick AGN candidates

One of the goals of this work is the identification of potential CT AGNs and studying the properties of their host galaxy in comparison with the overall properties of the type 2 AGN population. CT AGN show X-ray absorption with Hydrogen column densities $N_H > 10^{24} \text{ cm}^{-2}$ that largely suppress the direct X-ray emission below 10 keV (Ricci et al. 2015a,b; Georgantopoulos & Akylas 2019; Torres-Albà et al. 2021).

In order to identify CT candidates we follow the work of Pfeifle et al. (2022), where they presented a diagnostic for the X-ray absorption in AGN, based on the ratio of the mid-infrared and the 2 – 10 keV X-ray luminosities. As the mid-infrared luminosity represents a reliable proxy of the isotropic AGN emission, a low X-ray to mid-infrared luminosity ratio provides a powerful method to identify CT sources (Alexander et al. 2008; Georgantopoulos et al. 2011; Rovilos et al. 2014). Pfeifle et al. (2022) use the BAT AGN Spectroscopic Survey (BASS Koss et al. 2017; Koss et al. 2022; Ricci et al. 2017; Ichikawa et al. 2017) which includes sources detected in the ultrahard X-ray band (14–195 keV) and it is expected to be a complete census, independent of X-ray obscuration, of the most luminous AGN in the local Universe.

Using the same data set and methods of Pfeifle et al. (2022), we estimated the expected completeness and purity levels for CT samples using different X-ray-to-12- μm luminosity ratios, as shown in Fig. 1. Our results show that for $\log(L_{obs}(2 - 10 \text{ keV})/L(12 \mu\text{m})) < -1.6$ we can expect a ~ 80 per cent completeness with a purity of ~ 80 per cent.

We estimated the X-ray-to-12- μm luminosity ratios for our sample of low- z type 2 AGNs. Since this is a spectroscopically selected sample of nearby objects, it includes objects with low luminosity AGNs and the host galaxy emission dominates even in the MIR range. Hence, in order to avoid contamination due to the host galaxy, the 12 μm luminosity we used for estimating the Pfeifle et al. (2022) diagnostic is the corresponding to the AGN emission we obtained in our SED analysis using CIGALE (see Sect. 3.1).

Accordingly to the Pfeifle et al. (2022) diagnostic we discussed above, we considered CT candidates those sources below the $\log(L_{obs}(2 - 10 \text{ keV})/L(12 \mu\text{m})) = -1.6$ line and optically classified as Sy2 galaxies (see Fig. 2). We found a total of 14 CT candidates. Our CT sample is by no means complete. This is because we have discarded sources with low quality optical spectra i.e. signal to noise ratio lower than 10. Some CT sources especially the fainter ones may be among the discarded sources. In addition, our selected $\log(L_{obs}(2 - 10 \text{ keV})/L(12 \mu\text{m})) < -1.6$ criterion can find only 80% of the known CT AGN while among the selected CT AGN only 80% are bona-fide CT AGN. Finally, the low $\log(L_{obs}(2 - 10 \text{ keV})/L(12 \mu\text{m}))$ ratio criterion may be sensitive to other types of sources such as turnoff AGN, see for example the discussion in Saade et al. (2022).

Next we check in the literature whether our sources that have reasonably good quality X-ray observations available are associated indeed with CT AGN. Out of our 14 sources, three have been observed by *NuSTAR*: NGC 5765, IC2227 and LEDA 1373882. Masini et al. (2019) find that NGC 5765 is a reflection dominated CT AGN with $N_H \sim 10^{25} \text{ cm}^{-2}$. The *NuSTAR* observations of IC 2227 have been reported by Silver et al. (2022). They find that the source is heavily obscured with $N_H \sim$

Table 3: List of candidate Compton-thick sources

Name (1)	α (2)	δ (3)	redshift (4)	$F_{2-10\text{keV}}$ (5)	f_{AGN} (6)	Reference (7)
NGC5765	222.71464	5.11449	0.0279	1.6×10^{-13}	0.42	Masini et al. (2019)
2XMMJ121742.0+034632	184.42496	3.77529	0.0799	2.3×10^{-16}	0.75	
CGCG022-033	235.79429	1.32884	0.0397	4.9×10^{-14}	0.45	
IC 2227	121.77990	36.2330	0.0320	2.1×10^{-13}	0.33	Silver et al. (2022)
2MASSJ132904.5+560353	202.26895	56.06481	0.043	2.4×10^{-16}	0.07	
SDSSJ230231.1+000147	345.62978	0.02990	0.095	3.6×10^{-16}	0.60	
2MASSJ11435.6+153341	175.59826	15.5614	0.044	1.7×10^{-15}	0.28	
2MAXSJ141415.0+265812	213.56277	26.97002	0.066	1.3×10^{-14}	0.47	
2MASSJ145631.3+243635	224.13056	24.60972	0.033	2.5×10^{-14}	0.41	
WISEA J120749.5+251236.2	181.95637	25.21005	0.098	2.4×10^{-15}	0.43	
LEDA1593164	238.95164	11.40939	0.072	$< 5.8 \times 10^{-15}$	0.36	
MCG-02-05-022	24.27895	-9.14931	0.070	6.3×10^{-15}	0.63	
LEDA1373882	165.03945	10.05338	0.064	8.6×10^{-15}	0.77	
LEDA1169610	136.94548	0.57513	0.0536	2.3×10^{-15}	0.18	

Notes. (1): Name (2, 3): optical right ascension and declination [degrees]. (4): Spectroscopic redshift. (5): X-ray flux in the 2-10 keV band (erg s^{-1}). (6): AGN fraction according to the CIGALE spectral energy distribution fit. (7): Reference

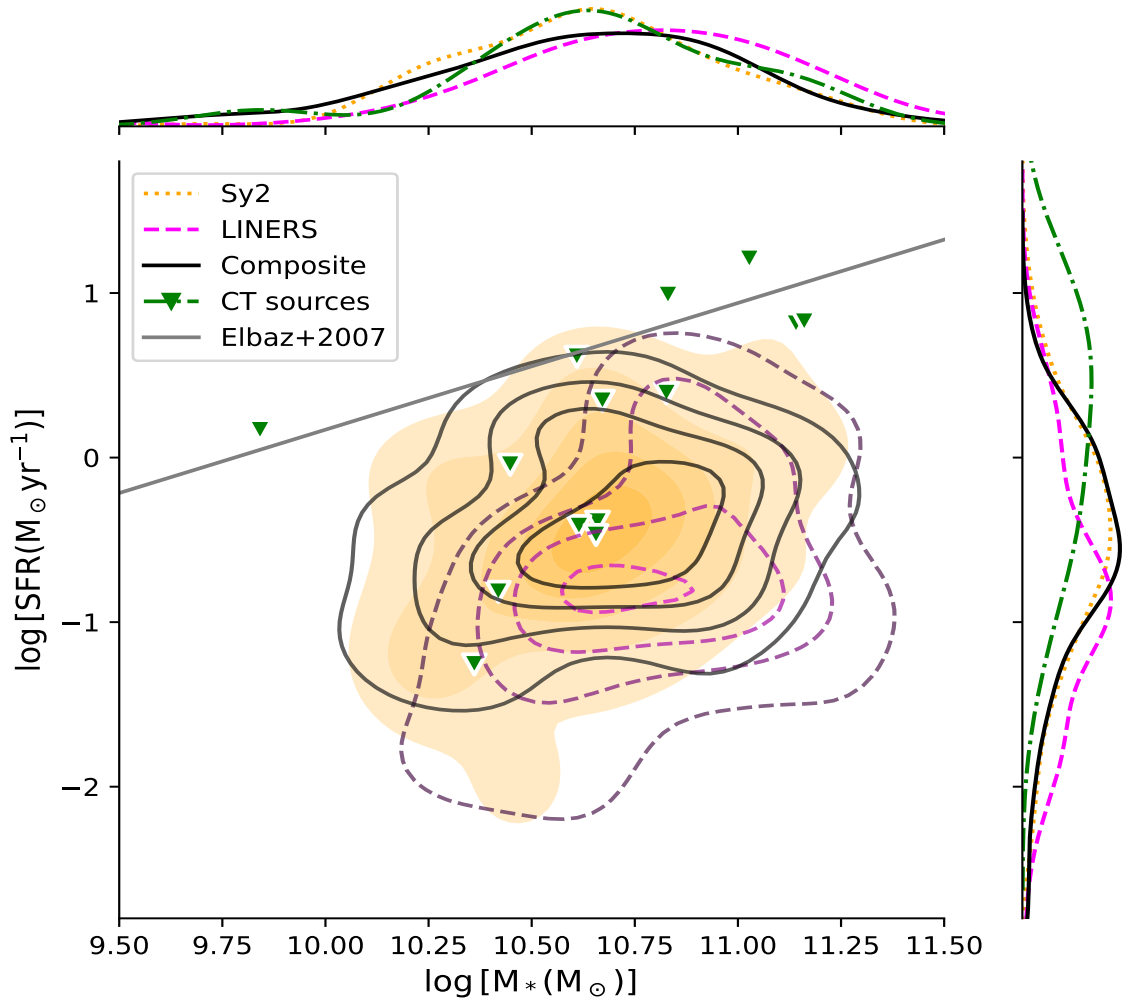


Fig. 3: Distribution of sources in the SFR- M_* plane. Different AGN populations are presented with different colours and lines, as indicated in the legend of the plot. The solid, grey line, shows the local SFR- M_* relation presented in Elbaz et al. (2007), for SDSS galaxies.

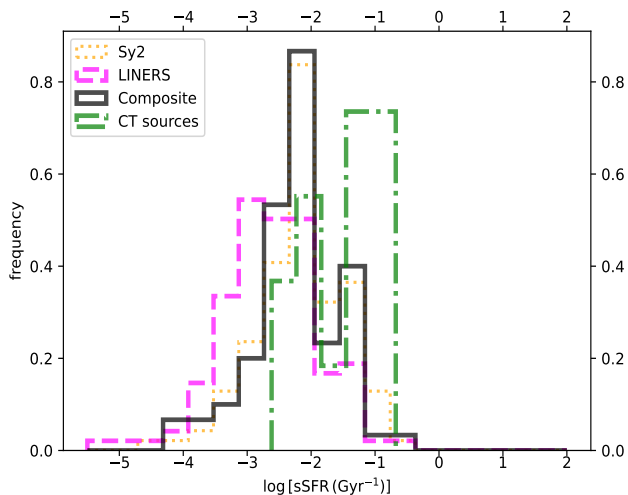


Fig. 4: The distribution of $s\text{SFR} \left(\frac{\text{SFR}}{M_*}\right)$ for the different AGN populations, used in our study.

$3 \times 10^{23} \text{cm}^{-2}$. The remaining source has not been detected by *NuSTAR*. Next, we search whether there is additional information in the literature regarding the X-ray spectra of the remaining 11 sources. The vast majority of these are faint sources, having fluxes below $5 \times 10^{-14} \text{erg cm}^{-2} \text{s}^{-1}$ thus impeding the extraction of good quality spectra. One of our candidate sources (LEDA1593164) has not been detected and there is only an upper limit in X-ray flux available (see e.g., Ruiz et al. 2021). Three of our sources are associated with targets: NGC5765, IC2227, and 2MASSX1390454+5603528. In Table 3 we give the full list of our CT candidate sources.

4. Results

In this section, we explore the location of diverse AGN populations in relation to the star-forming main-sequence (MS) and delve into the influence of SMBH activity on this location. Additionally, we conduct a comparison of their stellar populations and we analyze the accretion power exhibited by our sources.

4.1. The position of the AGN classes relative to the main-sequence

To examine the relative positioning of the different AGN populations in relation to the star-forming MS, we first investigate the distribution of our selected galaxies in the $\text{SFR}-M_*$ plane (Sect. 4.1.1) and then we compare the SFR of the sources in our dataset to the SFR of star-forming MS galaxies, as a function of luminosity (Sect. 4.1.2).

4.1.1. Distribution of sources in the $\text{SFR}-M_*$ plane

In Fig. 3, we illustrate the distribution of the AGN populations in the $\text{SFR}-M_*$ plane. Additionally, we incorporate the local $\text{SFR}-M_*$ relation, as determined from SDSS galaxies by Elbaz et al. (2007), represented by the grey line for reference. Notably, the majority of our sources appear below this line, indicating that our sources predominantly inhabit quiescent systems. Table 4 provides median values and their corresponding 25th and 75th percentiles for each host galaxy property and AGN class. Intriguingly,

LINERS galaxies exhibit the highest M_* (by ~ 0.2 dex) and the lowest SFR compared to other AGN classes. Among the four AGN classes, CT sources display the highest median SFR values. Despite these disparities, we note that Kolmogorov-Smirnov tests (KS-tests) indicate that these differences lack statistical significance (i.e., $< 2\sigma$), as the p -values obtained range from 0.2 – 0.9 (where a p -value = 0.05 signifies a statistical significance of $\sim 2\sigma$). Similar outcomes are observed with other statistical tests, such as Mann-Whitney, Anderson, and Kuiper tests.

Fig. 4 depicts the distributions of $s\text{SFR} \left(\frac{\text{SFR}}{M_*}\right)$ for different AGN classes, with median values and their corresponding 25th and 75th percentiles provided in Table 4. LINER galaxies exhibit the lowest $s\text{SFR}$ compared to other AGN populations, which display comparable median values and $s\text{SFR}$ distributions, with the exception of CT AGN that display the highest median $s\text{SFR}$ values. Notably, despite the p -values obtained from the comparison of LINERS' $s\text{SFR}$ distribution with other AGN populations being relatively lower (ranging from 0.1 – 0.2) compared to those for SFR and M_* distributions, these differences do not achieve statistical significance at a 2σ level.

4.1.2. SFR_{norm} vs. luminosity

An alternative way to illustrate the position of AGN relative to the MS, is to calculate the SFR_{norm} parameter (e.g., Mullaney et al. 2015; Masoura et al. 2018, 2021; Bernhard et al. 2019; Koutoulidis et al. 2022; Pouliasis et al. 2022; Mountrichas et al. 2022a, 2023; Mountrichas & Buat 2023). SFR_{norm} is defined as the ratio of the SFR of AGN to the SFR of star-forming MS galaxies, with comparable M_* and redshift. Therefore, $\text{SFR}_{\text{norm}} > 1$ indicates that the AGN is located above the MS, whereas $\text{SFR}_{\text{norm}} < 1$ indicate that the AGN is below the MS. For the calculation of SFR_{norm} , we utilize the expression derived in Elbaz et al. (2007), that used SDSS galaxies in the local Universe. It is important to note that using analytical expressions from existing literature for estimating SFR_{norm} may introduce systematic biases, as opposed to employing galaxy control samples (Mountrichas et al. 2021b). However, for the purposes of our analysis, these potential systematics do not impact our results and conclusions.

Fig. 5 presents the distribution of our sources in the $\text{SFR}_{\text{norm}} - \frac{L_{\text{SF}}}{L_{\text{AGN}}}$ space. L_{SF} and L_{AGN} are the luminosities originating from the star-formation and the AGN, respectively. Both parameters are defined as the integrated luminosities in the range between 8 and $1000 \mu\text{m}$. To gauge the accuracy of CIGALE's estimations for these parameters, we can check how well CIGALE calculates the AGN fraction, frac_{AGN} . This is because frac_{AGN} is defined as the fraction of the total infrared emission coming from the AGN and therefore is derived from data within similar wavelengths as these two parameters. In Fig. 6, we present the distributions of frac_{AGN} for the four AGN populations. This plot demonstrates the considerable range of AGN activity present in our sources. Sy2 and CT appear to have the highest frac_{AGN} values (median values of 0.28 and 0.44, respectively) compared to composite and LINER galaxies (median values of 0.14 and 0.17, respectively).

To evaluate the accuracy of frac_{AGN} , we use mock catalogues generated by CIGALE based on the best-fitting model for each source in our dataset. CIGALE essentially creates a mock sample by taking the best-fitting flux for each source and introducing noise to it, which is derived from a Gaussian distribution with the same standard deviation as the observed flux. The mock data

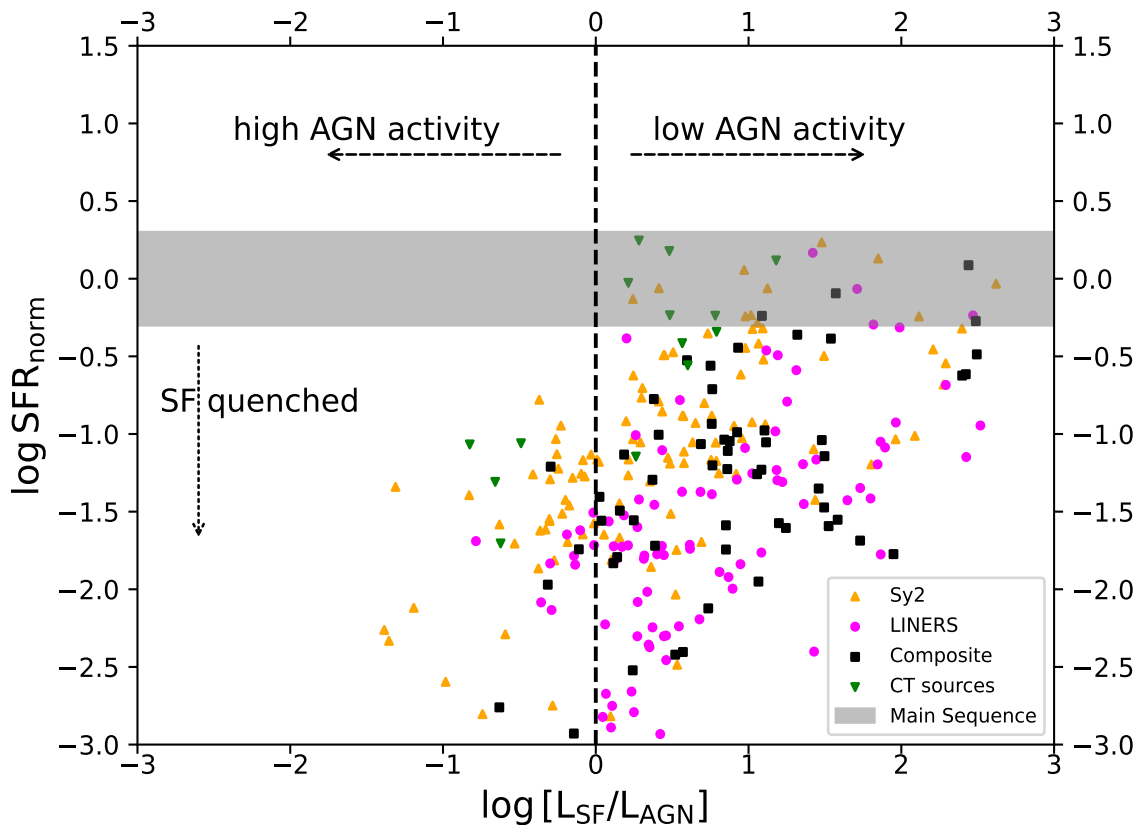


Fig. 5: SFR_{norm} as a function of the ratio of the star-formation luminosity (L_{SF}) to the AGN luminosity (L_{AGN}). SFR_{norm} is defined as the ratio of the SFR of the AGN to the SFR calculated using the Elbaz et al. (2007) expression for SDSS galaxies. The grey shaded area indicates an area ± 0.3 dex around $\log SFR_{norm} = 0$ to denote the main-sequence. Below the grey area, the star-formation of the AGN host galaxies is quenched. The dashed vertical lines indicates the $\log \frac{L_{SF}}{L_{AGN}} = 0$. At $\log \frac{L_{SF}}{L_{AGN}} < 0$ the AGN activity is the dominant mechanism in the host galaxy, whereas at $\log \frac{L_{SF}}{L_{AGN}} > 0$ the AGN activity is low.

Table 4: Median values and their 25th and 75th percentiles for the SFR, M_* , sSFR, D_n4000 , H_δ and λ_{sBHAR} of the different AGN populations examined in our study.

AGN population	$\log [SFR(M_\odot \text{yr}^{-1})]$	$\log [M_*(M_\odot)]$	$\log \text{sSFR}(\text{Gyr}^{-1})$	D_n4000	H_δ	$\log \lambda_{sBHAR}$
Sy2	-0.49 [-0.92, -0.03]	10.64 [10.41, 10.84]	-2.15 [-2.52, -1.75]	1.51 [1.39, 1.66]	0.35 [-1.15, 1.71]	-2.57 [-3.08, -2.26]
composite	-0.54 [-0.85, -0.08]	10.62 [10.42, 10.90]	-2.13 [-2.58, -1.92]	1.62 [1.50, 1.73]	0.50 [-0.77, 1.15]	-3.21 [-3.61, -2.78]
LINERS	-0.87 [-1.32, -0.36]	10.81 [10.56, 11.02]	-2.59 [-3.07, -2.15]	1.71 [1.53, 1.84]	-0.35 [-1.65, 1.45]	-3.28 [-3.69, -2.80]
CT	0.25 [-0.41, 0.76]	10.66 [10.49, 10.83]	-1.39 [-2.04, -1.08]	1.32 [1.18, 1.43]	1.69 [-0.44, 2.76]	-1.82 [-2.10, -1.60]

are then analyzed in the same manner as the actual observations. The precision of each estimated parameter can be assessed by comparing the original input values to the output values from the analysis (ground truth versus estimated value).

Our investigation revealed that the difference between the original and estimated values of the AGN fractions has a mean value of 0.05 (median value of 0.02), with a dispersion of 0.16. When we focus on sources with low AGN fraction values (less than 0.2), the mean difference is 0.04 (median difference is 0.03), with a dispersion of 0.08. Given these findings, we consider the calculated AGN fractions, and by extension the luminosities for star formation (L_{SF}) and active galactic nuclei (L_{AGN}), to be reliable.

Since we have addressed the reliability of the L_{SF} and L_{AGN} parameters, we now examine the distribution of our sources in the $SFR_{norm} - \frac{L_{SF}}{L_{AGN}}$ space (Fig. 5). In systems that have $\frac{L_{SF}}{L_{AGN}} < 1$ (or < 0 in logarithmic space) the AGN activity dominates over star-formation activity, while, $\frac{L_{SF}}{L_{AGN}} > 1$ implies either a more starburst-dominated galaxy or relatively low AGN luminosities (Netzer 2009). The grey shaded area indicates a ± 0.3 dex around the MS (i.e., around $SFR_{norm} = 1$). We notice that regardless of the AGN class, in all cases SFR_{norm} increases with $\frac{L_{SF}}{L_{AGN}}$, signifying that the AGN host galaxy is closer to the MS for higher values of $\frac{L_{SF}}{L_{AGN}}$. This trend could stem from either an elevation in L_{SF} , a reduction in L_{AGN} , or a combination of both factors as galaxies approach the MS. To discern the primary contributor of

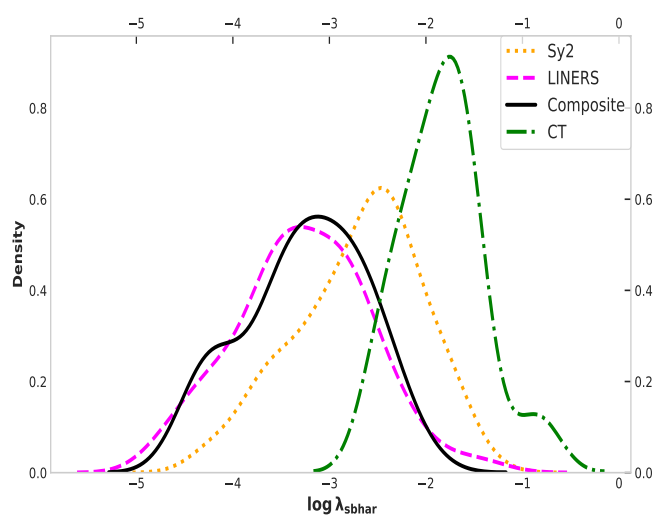
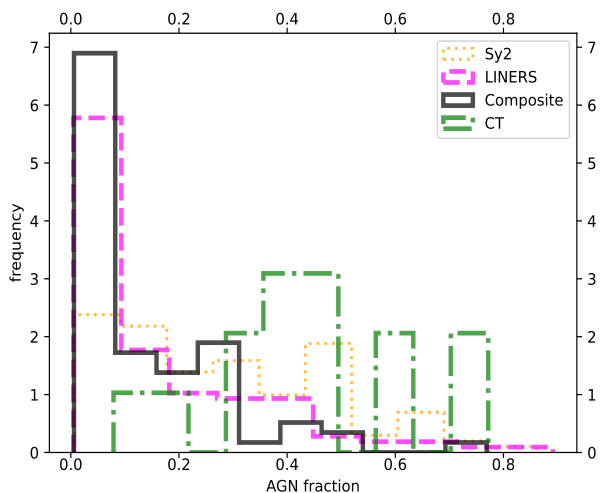


Fig. 6: Distributions of the AGN fractions, calculated by CIGALE, for the different AGN populations, as indicated in the legend. The AGN fraction is defined as the fraction of the total infrared emission coming from the AGN

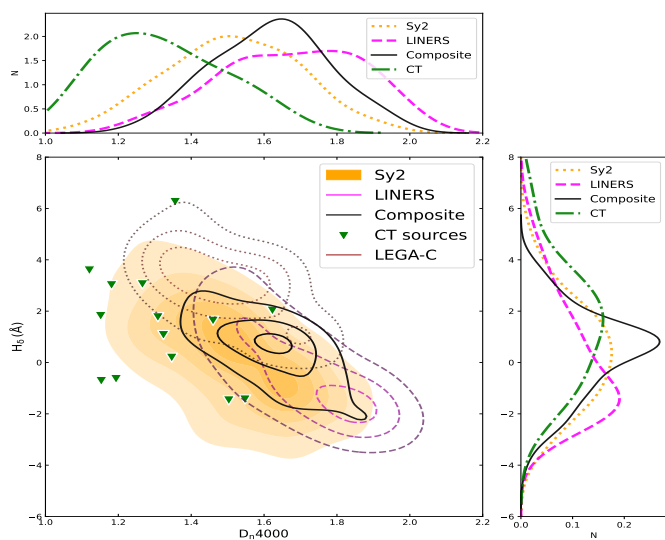


Fig. 7: Distribution of the different AGN populations in the H_δ – D_n4000 space. We also plot the results for the heavily obscured ($N_H > 10^{23} \text{ cm}^{-2}$) AGN sample used in [Georgantopoulos et al. \(2023\)](#), at $z \sim 1$ (LEGA-C, brown, dotted contours).

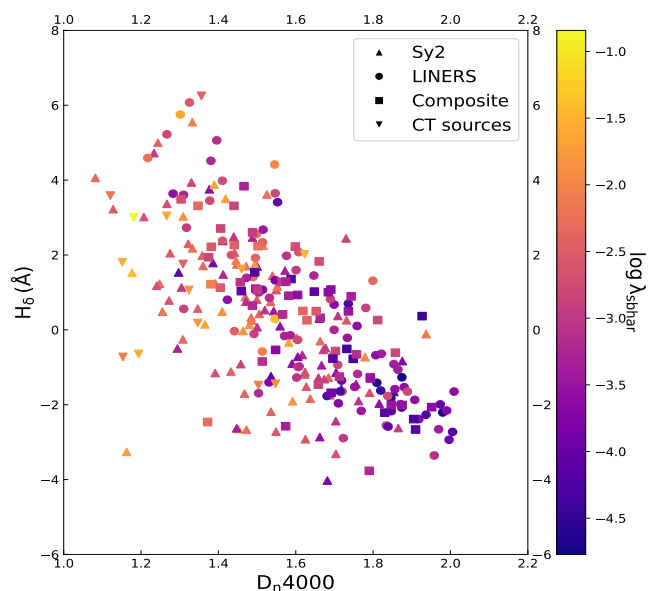


Fig. 8: The specific black hole accretion rate, λ_{sBHAR} , for the different AGN populations. The top panel shows the distribution of λ_{sBHAR} for the different AGN classes. The bottom panel shows the distribution of our sources in the H_δ – D_n4000 space, colour-coded based on their λ_{sBHAR} values.

what drives the AGN towards or away from the MS, we compute the slopes of the SFR– M_* relation for various AGN populations (see Fig. 3) using the linmix module (Kelly 2007). Linmix conducts a linear regression between two parameters by iteratively adjusting the data points within their uncertainties. The findings indicate that the slope gradually flattens as we transition from CT (slope of 1.24), to Sy2 (0.78), to composite (0.59), and ultimately to LINER galaxies (0.51). Therefore, AGN populations with higher AGN activity (based on their AGN fraction measurements, i.e., CT and Sy2) appear to have steeper slopes compared to AGN systems with lower AGN activity (i.e., composite and LINER galaxies). This may suggest that the AGN activity is aiding in quenching the SFR in the examined systems.

Overall, our analysis indicates that the majority of the sources examined in this study are positioned below the MS. LINERS preferentially inhabit galaxies characterized by higher stellar mass and lower levels of SFR activity compared to Sy2, composite, and CT sources. However, these distinctions do not reach statistical significance exceeding 2σ . We also find indications that CT sources may present enhanced levels of star-formation compared to non-CT AGN. Additionally, our results suggest that a lower level of AGN activity corresponds to a closer positioning of the host galaxy to the MS.

4.2. The stellar populations of the different AGN classes

Next, we conduct a comparative analysis of the stellar populations among galaxies hosting different AGN classes. In Fig. 7, we illustrate the distributions of the various AGN populations in the H_δ - D_n4000 space. Recognizing that more massive systems tend to harbor older stars, we apply weights to these distributions based on the M_* of the sources. Specifically, we assign a weight to each AGN to match the M_* of the four AGN classes (e.g. Mountrichas et al. 2022b). It is important to highlight that, while the D_n4000 measurements exhibit relatively small uncertainties (with a median uncertainty value representing approximately 10% of the measured value), the uncertainties associated with H_δ are notably larger (with a median value of H_δ uncertainties being around 80% of the measured value). Consequently, while we provide the distributions of the H_δ spectral line, our primary conclusions are derived from the results based on the D_n4000 spectral index due to its comparatively smaller errors.

Our findings indicate that LINER galaxies exhibit, on average, the oldest stellar populations compared to the other AGN classes. Sy2 and composite galaxies display stars of similar age, while CT sources showcase the youngest stars among the various AGN classes examined in our study. Although the statistical tests do not reveal significant differences based on the calculated p - values, likely due to the broad distributions, the observed patterns in the distributions are notably distinct. The median values along with their corresponding 25th and 75th percentiles for each galaxy population are presented in Table 4.

These findings align with the outcomes presented in the previous section. Specifically, LINER galaxies, characterized by the lowest star-formation activity among the various AGN classes, demonstrate the highest D_n4000 values, indicating they harbor the oldest stellar populations. Composite and Sy2 galaxies, which share similar levels of star-formation activity, also tend to possess comparable stellar populations. Furthermore, our current results are consistent with those in the prior section, underscoring that CT sources, on average, display heightened star-formation activity and host the youngest stellar populations among the AGN classes examined in this study.

In Fig. 7, we also juxtapose the distribution of our sources in the H_δ - D_n4000 space with that of the heavily obscured LEGA-C AGN, as presented in Georgantopoulos et al. (2023) (illustrated by brown, dotted contours). In the study by Georgantopoulos et al. (2023), 73 AGN in the COSMOS field were examined, with available measurements for their spectral indices obtained from the LEGA-C catalogue (van der Wel et al. 2021) at redshifts within $0.6 < z < 1$. The investigation involved a comparison of various properties, including M_* , sSFR, Eddington ratio, and stellar populations, between heavily obscured and non-obscured AGN, using X-ray criteria for the classification of the sources and applying a threshold at $N_H = 10^{23} \text{ cm}^{-2}$. Notably, the LEGA-C AGN exhibit lower D_n4000 values (and higher H_δ values) compared to our sample. It is crucial to acknowledge that the two AGN populations differ not only in terms of their redshifts but also in their classification criteria, their M_* properties (see bottom panel of Fig. 4) and L_X (LEGA-C AGN are about two orders of magnitude more luminous compared to the sources used in our analysis; see also the discussion in Sect. 5).

4.3. The accretion efficiency of different AGN classes

In this section, we investigate the accretion efficiency across various AGN classes within our datasets. This efficiency is measured through the n_{Edd} . In cases where the M_{BH} measurements

are not available, the specific black hole accretion rate, λ_{sBHAR} , is used as a proxy of the n_{Edd} (e.g., Aird et al. 2018; Mountrichas et al. 2021b, 2022c). For the calculation of λ_{sBHAR} the following expression is used:

$$\lambda_{sBHAR} = \frac{L_{bol}}{1.26 \times 10^{38} \text{ erg s}^{-1} \times 0.002 \frac{M_*}{M_\odot}}. \quad (1)$$

To calculate λ_{sBHAR} , we employ the measurements of L_{bol} and M_* provided by CIGALE. It is important to acknowledge that the effectiveness of λ_{sBHAR} as a proxy for n_{Edd} hinges on factors such as the scatter in the M_{BH} - M_* relation and the accuracy of AGN bolometric luminosity estimates, as previous studies have shown (Lopez et al. 2023; Mountrichas & Buat 2023). Nonetheless, in our examination, we emphasize the comparison of λ_{sBHAR} across distinct AGN classes rather than its absolute values.

Figure 8 displays the distributions of λ_{sBHAR} for various AGN populations in our dataset (top panel). The corresponding median values and percentiles are shown in Table 4. Our findings indicate that LINER and composite galaxies showcase analogous λ_{sBHAR} distributions and median values, which are also the lowest among the AGN classes considered. Sy2 galaxies tend to exhibit higher λ_{sBHAR} values, while CT sources present the highest λ_{sBHAR} values within the AGN populations in our sample. Utilizing the KS-test indicates that these distinctions hold statistical significance at a level exceeding $> 2\sigma$, as the p - values range from 10^{-5} to 10^{-7} . Comparable p - values are obtained through other statistical tests, including Mann-Whitney, Anderson, and Kuiper.

The bottom panel of Figure 8, presents the distribution of the different AGN classes in the H_δ - D_n4000 space, colour-coded based on the λ_{sBHAR} of the sources. The results indicate that sources with younger stellar populations (i.e., $D_n4000 < 1.4$) tend to exhibit higher λ_{sBHAR} values compared to sources with older stars. This is in line with the findings of Georgantopoulos et al. (2023, see their Fig. 4).

5. Discussion

In this work, we have identified CT sources and have investigated their properties as a different AGN class and compare it with the other AGN populations. We found indications that CT sources may present enhanced levels of star-formation activity, but, most importantly, our analysis revealed that CT sources are hosted by galaxies that have the youngest stellar population and their SMBH present the highest accretion efficient across the different AGN classes. Georgantopoulos et al. (2023) used AGN in the COSMOS field and found that highly obscured sources ($N_H > 10^{23} \text{ cm}^{-2}$) live in galaxies with older stars (higher D_n4000 values) compared to their unobscured (or moderately obscured) counterparts. Their analysis also showed that highly obscured AGN have lower n_{Edd} compared to unobscured sources.

It is important to note, though, that our sample has significant differences compared to that used in Georgantopoulos et al. (2023). In Georgantopoulos et al. (2023) the classification of sources is based on X-ray criteria, as opposed to the optically classified sources employed in our work. Previous works have shown that the two classification schemes do not necessarily coincide (e.g., Merloni et al. 2014; Li et al. 2019; Masoura et al. 2020). Furthermore, our dataset spans significantly lower X-ray luminosities (the majority of our sources have $\log [L_{X,2-10\text{keV}}(\text{ergs}^{-1})] < 42$) compared to the luminosities

probed by the COSMOS sample that is used in [Georgantopoulos et al. \(2023\)](#), where $42.5 < \log [L_{X,2-10\text{keV}}(\text{ergs}^{-1})] < 44.3$. Moreover, the galaxies employed in the [Georgantopoulos et al. \(2023\)](#) analysis are more massive compared to our galaxies, with a median difference of ~ 0.7 dex. Therefore, apart from the redshift difference between the two datasets, most likely, the two studies probe different AGN populations which may have been triggered by different physical processes. Previous studies have also suggested that the comparison of the SFR of (X-ray or optically selected) obscured and unobscured AGN differs as a function of redshift and L_X (e.g., [Mountrichas & Georgantopoulos 2024](#); [Mountrichas et al. 2024b,a](#)).

Our results also show higher λ_{sBHAR} values for Sy2 galaxies compared to Composite and LINERS. Previous studies found that type 1 AGN exhibit elevated λ_{sBHAR} values in comparison to type 2 (e.g., [Mountrichas & Georgantopoulos 2024](#)). Similar outcomes have been observed when the AGN classification is based on X-ray criteria (e.g. [Ricci et al. 2017, 2022](#); [Georgantopoulos et al. 2023](#); [Ricci et al. 2023](#); [Mountrichas et al. 2024b](#)). The higher λ_{sBHAR} values of type 1/unobscured AGN compared to type 2/obscured has been attributed to the effect of radiation pressure. Specifically, at higher Eddington ratios, radiation pressure may lead to a reduction in the covering factor of obscuring gas, making sources more likely to be observed as unobscured ([Ricci et al. 2017](#)). Our analysis also incorporates CT sources, which exhibit the highest λ_{sBHAR} values among the four AGN classes examined in this study. In Fig. 3 and the extended data Fig. 1 of [Ricci et al. \(2017\)](#), there is a suggestion of elevated λ_{sBHAR} values for CT sources compared to Compton-thin AGN ($N_H = 10^{22-24} \text{ cm}^{-2}$). High λ_{sBHAR} values for CT AGN were also reported by [Brightman et al. \(2016\)](#) ($\log \lambda_{sBHAR} \sim -1$), using 12 megamaser AGN detected by *NuSTAR*.

In a study by [Leslie et al. \(2016\)](#), they employed data from the SDSS data release 7, utilizing properties calculated by the MPA/JHU group. It is worth noting that their methods for computing host galaxy properties differ from our SED fitting analysis. Their investigation revealed that composite, Seyfert, and LINER galaxies are positioned below the main sequence, emphasizing the substantial impact of AGN activity in suppressing star-formation in these systems. Moreover, based on their findings LINERS have, on average, the lowest SFR and the highest M_* , among the different AGN populations. Our results align remarkably well with their observations.

In an investigation conducted by [Kewley et al. \(2006\)](#), they focused on 85 224 emission-line galaxies selected from SDSS and identified a significant distinction between Seyferts and LINERS, particularly in terms of their n_{Edd} . Their analysis indicated that LINERS tend to exhibit predominantly lower n_{Edd} values compared to Sy2 galaxies. Our results align with these observations. Additionally, their investigation into the stellar populations of different AGN classes, based on the distributions of the D4000 spectral index, revealed that LINER galaxies have older stellar populations (higher D4000 values) compared to Seyferts. Once again, our findings are consistent with these outcomes.

Our results could indicate that the different types of AGN we have examined may result from distinct phases of AGN activity. For example, if a SMBH becomes active early in a galaxy's evolution, when there is plenty of gas, it might exhibit a high accretion rate, appearing as a Sy2 and potentially transitioning from CT to Sy2. On the other hand, if the AGN activity begins later in the galaxy's timeline when gas is less abundant, the SMBH would likely have a lower accretion rate, leading to a LINER (e.g., [Torres-Papaqui et al. 2024](#)).

6. Conclusions

In this work, we used 338 galaxies at $0.02 < z < 0.1$ to study the AGN and host galaxy properties of different (non-QSO) AGN classes included in the SDSS-DR18 catalogue. These sources have available classification that is based on their emission-line ratios. Specifically, galaxies are classified into Sy2, composite and LINERS. Among these sources, we identified and select CT AGN, using their $L_X-L_{12\mu\text{m}}$ relation ([Asmus et al. 2014](#)) and applying the threshold suggested by [Pfeifle et al. \(2022\)](#). We constructed and fit the SED of the sources using the CIGALE code and applied strict criteria to include in our analysis only sources with reliable SED fitting measurements. Our sample consists of 118 Sy2, 82 composite, 124 LINERS and 14 CT sources. The 14 CT AGN are classified as Sy2 and have been excluded from the Sy2 populations. These sources have available measurements for their D_n4000 and H_δ spectral indices, which serve as proxies for their stellar populations. Our goal was to examine the position of these AGN populations relative to the main-sequence, compare their stellar populations and their accretion efficiency. Our main findings are summarized as follows:

- The majority of sources, regardless of their classification, are situated below the main-sequence. LINERS predominantly reside in galaxies characterized by higher stellar mass and lower levels of star formation activity compared to Sy2, composite, and CT sources.
- Our findings suggest that a lower level of AGN activity corresponds to a closer alignment of the host galaxy with the main-sequence.
- When comparing their spectral indices, LINERS exhibit the oldest stellar populations (indicated by higher D_n4000 values) compared to other AGN populations. Composite and Sy2 galaxies show similar stellar populations, while CT AGN host the youngest stellar populations among the classes examined in this study.
- In LINER and composite galaxies the AGN displays the lowest accretion efficiency (lower specific black hole accretion values), while CT AGN, on average, exhibit the most efficient accretion among the four AGN populations.

In summary, our comprehensive analysis sheds light on the diverse characteristics of AGN host galaxies, emphasizing the intricate interplay between AGN activity, stellar populations, and accretion efficiency. These insights contribute to a deeper understanding of the multifaceted nature of AGN and their impact on host galaxy properties.

Acknowledgements. This project has received funding from the European Union's Horizon 2020 research and innovation program under grant agreement no. 101004168, the XMM2ATHENA project.

References

- Aird, J., Coil, A. L., & Georgakakis, A. 2018, *Monthly Notices of the Royal Astronomical Society*, 474, 1225
- Alexander, D. M., Chary, R. R., Pope, A., et al. 2008, *ApJ*, 687, 835
- Almeida, A., Anderson, S. F., Argudo-Fernández, M., et al. 2023, *ApJS*, 267, 44
- Asmus, D., Hönig, S. F., Gandhi, P., Smette, A., & Duschl, W. J. 2014, *Monthly Notices of the Royal Astronomical Society*, 439, 1648
- Bernhard, E., Grimmert, L. P., Mullaney, J. R., et al. 2019, *Monthly Notices of the Royal Astronomical Society: Letters*, 483, L52
- Bianchi, L., Shiao, B., & Thilker, D. 2017, *ApJS*, 230, 24
- Boquien, M., Burgarella, D., Roehlly, Y., et al. 2019, *Astronomy & Astrophysics*, 622, A103
- Brightman, M., Masini, A., Ballantyne, D. R., et al. 2016, *The Astrophysical Journal*, 826, 93

- Bruzual, G. & Charlot, S. 2003, *MNRAS*, 344, 1000
- Buat, V., Ciesla, L., Boquien, M., Małek, K., & Burgarella, D. 2019, *Astronomy & Astrophysics*, 632, A79
- Buat, V., Mountrichas, G., Yang, G., et al. 2021, *A&A*, 654, A93
- Charlot, S. & Fall, S. M. 2000, *ApJ*, 539, 718
- Constantin, A. & Vogeley, M. S. 2006, *The Astrophysical Journal*, 650, 727
- Cutri, R. M., Wright, E. L., Conrow, T., et al. 2013, Explanatory Supplement to the AllWISE Data Release Products, Explanatory Supplement to the AllWISE Data Release Products, by R. M. Cutri et al.
- Dale, D. A., Helou, G., Magdis, G. E., et al. 2014, *ApJ*, 784, 83
- Elbaz, D., Daddi, E., Borgne, D. L., et al. 2007, *Astronomy & Astrophysics*, 468, 33
- Georgantopoulos, I. & Akylas, A. 2019, *A&A*, 621, A28
- Georgantopoulos, I., Pouliaxis, E., Mountrichas, G., et al. 2023, *Astronomy & Astrophysics*, 673, A67
- Georgantopoulos, I. et al. 2011, *A&A*, 534, 23
- Heckman, T. M. & Best, P. N. 2014, *Annual Review of Astronomy and Astrophysics*, 52, 589
- Ichikawa, K., Ricci, C., Ueda, Y., et al. 2017, *ApJ*, 835, 74
- Kauffmann, G., Heckman, T. M., White, D. M. S., et al. 2003, *Monthly Notices of the Royal Astronomical Society*, 341, 33
- Kauffmann, G., Heckman, T. M., White, S. D. M., et al. 2003, *MNRAS*, 341, 54
- Kelly, B. C. 2007, *The Astrophysical Journal*, 665, 1489
- Kewley, L. J., Groves, B., Kauffmann, G., & Heckman, T. 2006, *Monthly Notices of the Royal Astronomical Society*, 372, 961
- Koss, M., Trakhtenbrot, B., Ricci, C., et al. 2017, *The Astrophysical Journal*, 850, 74
- Koss, M. J., Ricci, C., Trakhtenbrot, B., et al. 2022, *ApJS*, 261, 2
- Koutoulidis, L., Mountrichas, G., Georgantopoulos, I., Pouliaxis, E., & Plionis, M. 2022, *Astronomy & Astrophysics*, 658, A35
- Lawrence, A. et al. 2007, *MNRAS*, 379, 1599
- Leslie, S. K., Kewley, L. J., Sanders, D. B., & Lee, N. 2016, *Monthly Notices of the Royal Astronomical Society: Letters*, 455, L82
- Li, J., Xue, Y., Sun, M., et al. 2019, *The Astrophysical Journal*, 877, 5
- Lopez, I. E., Brusa, M., Bonoli, S., et al. 2023, *Astronomy & Astrophysics*, 672, A137
- Małek, K., Buat, V., Roehly, Y., et al. 2018, *Astronomy & Astrophysics*, 620, A50
- Masini, A., Comastri, A., Hickox, R. C., et al. 2019, *ApJ*, 882, 83
- Masoura, V. A., Georgantopoulos, I., Mountrichas, G., et al. 2020, *Astronomy & Astrophysics*, 638, A45
- Masoura, V. A., Mountrichas, G., Georgantopoulos, I., & Plionis, M. 2021, *Astronomy & Astrophysics*, 646, A167
- Masoura, V. A., Mountrichas, G., Georgantopoulos, I., et al. 2018, *A&A*, 618, 31
- Merloni, A., Bongiorno, A., Brusa, M., et al. 2014, *Monthly Notices of the Royal Astronomical Society*, 437, 3550
- Mountrichas, G. & Buat, V. 2023, *Astronomy & Astrophysics*, 679, A151
- Mountrichas, G., Buat, V., Georgantopoulos, I., et al. 2021a, *Astronomy & Astrophysics*, 653, A70
- Mountrichas, G., Buat, V., Yang, G., et al. 2021b, *Astronomy & Astrophysics*, 653, A74
- Mountrichas, G., Buat, V., Yang, G., et al. 2022a, *Astronomy & Astrophysics*, 663, A130
- Mountrichas, G., Buat, V., Yang, G., et al. 2022b, *Astronomy & Astrophysics*, 667, A145
- Mountrichas, G. & Georgantopoulos, I. 2024, *Astronomy & Astrophysics*, 683, A160
- Mountrichas, G., Masoura, V. A., Corral, A., & Carrera, F. J. 2024a, *Astronomy & Astrophysics*, 683, A143
- Mountrichas, G., Masoura, V. A., Xilouris, E. M., et al. 2022c, *Astronomy & Astrophysics*, 661, A108
- Mountrichas, G., Viitanen, A., Carrera, F. J., et al. 2024b, *Astronomy & Astrophysics*, 683, A172
- Mountrichas, G., Yang, G., Buat, V., et al. 2023, *Astronomy & Astrophysics*, 675, A137
- Mullaney, J. R., Alexander, D. M., Aird, J., et al. 2015, *Monthly Notices of the Royal Astronomical Society: Letters*, 453, L83
- Netzer, H. 2009, *Monthly Notices of the Royal Astronomical Society*, 399, 1907
- Pfeifle, R. W., Ricci, C., Boorman, P. G., et al. 2022, *The Astrophysical Journal Supplement Series*, 261, 3
- Pouliaxis, E., Mountrichas, G., Georgantopoulos, I., et al. 2022, *Astronomy & Astrophysics*, 667, A56
- Ricci, C., Ananna, T. T., Temple, M. J., et al. 2022, *The Astrophysical Journal*, 938, 67
- Ricci, C., Ichikawa, K., Stalevski, M., et al. 2023, *The Astrophysical Journal*, 959, 27
- Ricci, C., Trakhtenbrot, B., Koss, M. J., et al. 2017, *ApJS*, 233, 17
- Ricci, C., Trakhtenbrot, B., Koss, M. J., et al. 2017, *Nature*, 549, 488
- Ricci, C., Ueda, Y., Koss, M. J., et al. 2015a, *ApJ*, 815, L13
- Ricci, C., Ueda, Y., Koss, M. J., et al. 2015b, *ApJ*, 815, L13
- Rosario, D. J., Trakhtenbrot, B., Lutz, D., et al. 2013, *Astronomy & Astrophysics*, 560, A72
- Rosario, D. J. et al. 2012, *A&A*, 545, 18
- Rovilos, E., Georgantopoulos, I., Akylas, A., et al. 2014, *MNRAS*, 438, 494
- Ruiz, A., Georgakakis, A., Gerakakis, S., et al. 2022, *MNRAS*, 511, 4265
- Ruiz, A., Georgantopoulos, I., & Corral, A. 2021, *Astronomy & Astrophysics*, 645, A74
- Saade, M. L., Brightman, M., Stern, D., Malkan, M. A., & García, J. A. 2022, *ApJ*, 936, 162
- Santini, P., Rosario, D. J., Shao, L., et al. 2012, *Astronomy & Astrophysics*, 540, A109
- Silver, R., Torres-Albà, N., Zhao, X., et al. 2022, *ApJ*, 940, 148
- Skrutskie, M. F., Cutri, R. M., Stiening, R., et al. 2006, *AJ*, 131, 1163
- Smolčić, V. 2009, *The Astrophysical Journal*, 699, L43–L47
- Stalevski, M., Fritz, J., Baes, M., Nakos, T., & Popović, L. Č. 2012, *Monthly Notices of the Royal Astronomical Society*, 420, 2756
- Stalevski, M., Ricci, C., Ueda, Y., et al. 2016, *Monthly Notices of the Royal Astronomical Society*, 458, 2288
- Thomas, D., Steele, O., Maraston, C., et al. 2013, *MNRAS*, 431, 1383
- Torres-Albà, N., Marchesi, S., Zhao, X., et al. 2021, *ApJ*, 922, 252
- Torres-Papaqui, J. P., Coziol, R., Robledo-Orus, A. C., Cutiva-Alvarez, K. A., & Roco-Avilez, P. 2024, *AJ*, submitted [arXiv:2405.05184]
- van der Wel, A., Bezanson, R., D'Eugenio, F., et al. 2021, *The Astrophysical Journal Supplement Series*, 256, 44
- Villa-Velez, J. A., Buat, V., Theule, P., Boquien, M., & Burgarella, D. 2021, *Astronomy & Astrophysics*, 654, A153
- Webb, N. A., Coriat, M., Traulsen, I., et al. 2020, *A&A*, 641, A136
- Yang, G., Boquien, M., Brandt, W. N., et al. 2022, *The Astrophysical Journal*, 927, 192
- Yang, G., Boquien, M., Buat, V., et al. 2020, *Monthly Notices of the Royal Astronomical Society*, 491, 740
- Zhang, X. 2023, *ApJS*, 267, 36